Enhanced photocatalytic activity of hierarchical structure TiO2 hollow spheres with reactive (001) facets for the removal of toxic heavy metal Cr(VI)

ARTICLE *in* RSC ADVANCES · JULY 2014

Impact Factor: 3.84 · DOI: 10.1039/C4RA04787G

RSC Advances

PAPER

Cite this: *RSC Adv.*, 2014, **4**, 34577

Enhanced photocatalytic activity of hierarchical structure TiO_2 hollow spheres with reactive (001) facets for the removal of toxic heavy metal Cr(VI)†

Yong Yang,[a] Guozhong Wang,*[a] Quan Deng,[a] Huiming Wang,[a] Yunxia Zhang,[a] Dickon H. L. Ng[b] and Huijun Zhao[ac]

Received 21st May 2014
Accepted 22nd July 2014

DOI: 10.1039/c4ra04787g

www.rsc.org/advances

Hierarchical structure TiO_2 hollow spheres composed of nanometer-sized building blocks, nanoflakes with exposed anatase (001) facets, have been synthesized with a high yield through a facile fluoride-mediated hydrothermal route. The average diameter of the resultant TiO_2 hollow spheres is ~1 μm, and the width of well-crystallized anatase phase nanoflakes is ~50 nm. Nitrogen adsorption–desorption measurement revealed that the products have a high specific surface area of 26 m^2 g^{-1} and abundant mesoporous structure. The TiO_2 hollow spheres were used to photocatalytically degrade Cr(VI) in solution. The results indicate an enhanced photocatalytic activity compared to other TiO_2 structures, owing to the high specific surface area and abundant mesoporous properties of the TiO_2 hollow spheres. Besides, the presence of the reactive (001) facets also contributed to the enhanced activity; it was found that the (001) facets are more effective in the adsorption of Cr(VI) than the commonly exposed (101) facets. Furthermore, the surface fluorination of TiO_2 hollow spheres was found to have a negative role in the photocatalytic removal of Cr(VI). The TiO_2 hollow spheres not only can remove Cr(VI) from wastewater; they also can reduce the adsorbed toxic Cr(VI) to Cr(III), further forming oxides or hydroxides. In addition, the TiO_2 hollow sphere photocatalysts with micron-scale size showed high durability in the cyclic tests.

Introduction

Water pollution caused by heavy metal ions has drawn extensive attention; among the heavy metals, Cr(VI) is particularly hazardous owing to its acute toxicity to humans and its high mobility in water.[1–6] Various techniques have been used to treat Cr(VI) contamination, including ion exchange,[7] electrocoagulation,[8,9] membrane separation,[10] adsorption,[11,12] and photocatalytic reduction.[13–15] Among these methods, ion exchange and membrane separation methods are not attractive because of their high operating costs, complicated procedures and harsh conditions. Electrocoagulation and adsorption methods are only able to transfer Cr(VI) but not effectively degrade its toxicity; these must be followed by secondary treatments.[16] Heterogeneous photocatalytic reduction using the semiconductor photocatalyst TiO_2 has been proposed as an economical and simple method for the removal of Cr(VI), especially when it is present in low concentrations.[13–15]

Structural modification of the TiO_2 photocatalyst has been demonstrated to be an effective way to improve its photocatalytic activity. Among different TiO_2 structures (including nanoparticles, nanorods, and nanosheets), the TiO_2 hollow sphere structure has received considerable attention due to its low density, large surface area, good surface permeability, and greater light-harvesting capacity.[17,18] It has been reported that the TiO_2 hollow spheres show enhanced photocatalytic activity, compared to the commercially available nanometer-sized TiO_2 powders, in the photodegradation of organic pollutants such as acetone,[17,19] rhodamine B,[20] methyl orange[18] and the brilliant Red X3B.[21] The spheres' high specific surface area and abundant mesoporous properties contributed to the enhanced photocatalytic activity; also, the micron meter sizes facilitated the recovery of the catalysts and provided great value in practical use.

On the other hand, the synthesis of reactive (001) facet-exposed anatase TiO_2 single crystals has also been proven to be an alternative route to improve the photocatalytic efficiency of photocatalysts.[22–24] Numerous studies have suggested that the reactive (001) facets show considerably enhanced photocatalytic activity towards the photocatalytic oxidation of organic pollutants. However, most researchers focused on the photocatalytic

[a]*Key Laboratory of Materials Physics, Centre for Environmental and Energy Nanomaterials, Anhui Key Laboratory of Nanomaterials and Nanotechnology, Institute of Solid State Physics, Chinese Academy of Sciences, P.O. Box 1129, Hefei 230031, P.R. China. E-mail: gzhwang@issp.ac.cn; Fax: +86 0551 65591434; Tel: +86 0551 65595616*

[b]*Department of Physics, The Chinese University of Hong Kong, Shatin, Hong Kong, P.R. China*

[c]*Centre for Clean Environment and Energy, Gold Coast Campus, Griffith University, Queensland 4222, Australia*

† Electronic supplementary information (ESI) available: Additional figures including FESEM image, optical absorbance spectra, TEM image, XPS spectra, and so on. See DOI: 10.1039/c4ra04787g

activity of the TiO_2 hollow spheres or the reactive (001) facets for the photodegradation of organic pollutants;[17–24] little attention has been paid to the photocatalytic reduction removal of the toxic heavy metal Cr(VI). The structural advantages of TiO_2 hollow spheres and reactive (001) facets should be expected to show a great potential in the photocatalytic reduction removal of Cr(VI). He *et al.* reported the use of reactive (001) facet-exposed anatase TiO_2 nanosheets for the photocatalytic removal of Cr(VI), and enhanced activity was demonstrated;[25] however, the nanosheets tended to overlap with each other during the liquid phase photocatalysis, resulting in undesirable reduction in the specific surface area. It would be attractive to assemble the reactive (001) facet-exposed TiO_2 nanosheets into micrometer-sized hierarchical hollow sphere structures and use them for the photocatalytic reduction removal of the toxic heavy metal Cr(VI).

As to the synthesis of TiO_2 hollow sphere structures with reactive (001) facets, great efforts have been made by researchers;[18,26,27] however, most reported methods of synthesis either involve multiple complex reaction steps or require the use of extremely corrosive and toxic raw materials, such as hydrofluoric acid. Here, we report the synthesis of micron-sized hierarchical structure TiO_2 hollow spheres with reactive (001) facets based on a facile fluoride-mediated strategy. The photocatalytic activity and durability of the TiO_2 hollow spheres in the removal of Cr(VI) are reported for the first time; the influence of surface fluorination and reactive (001) facets on the photocatalytic activity are also investigated and discussed in detail.

Experimental section

Sample preparation

All reagents were commercial and used without further purification. Deionized water was used in the experiments. In a typical synthesis, 2 mmol of titanium sulfate ($Ti(SO_4)_2$, $\geq$ 96.0%, Shang Hai Nan Hui Chemical Reagent Co. Ltd, CP) was dissolved into a 40 mL mixed solution of ammonium fluoride (NH_4F, Wu Xi Zhan Wang Chemical Reagent Co. Ltd, AR) and deionized water, then stirred for 3 h at room temperature. The molar ratio of fluorine to titanium (R_F) was 3, *i.e.* 6 mmol of NH_4F was used. The mixed solution was transferred to a 70 mL Teflon-lined autoclave and maintained at 180 °C for 10 h. The white precipitates were collected, washed and rinsed with deionized water and ethanol, respectively, then dried in the oven at 70 °C for 8 h. The product was denoted as F-THS. The TiO_2 hollow spheres composed of smaller crystallite sizes (denoted as SF-THS) were synthesized using a process similar to the above, with the addition of 4 mmol urea into the reaction solution, according to previous work.[16] To remove the adsorbed fluorine ions on the surface of TiO_2, the sample was soaked in 0.1 M NaOH solution for 1 h and rinsed several times with deionized water until the pH value of the supernatant had attained a reading close to 7. The sample was then dried in an oven at 70 °C for 8 h. The samples of F-THS and SF-THS after removal of the adsorbed fluorine ions from the surface were denoted as THS and S-THS, respectively.

Characterization

The phases of the products were identified by X-ray diffraction analysis (XRD, Philips X'pert PRO) using Ni-filtered monochromatic CuK_α radiation at 40 keV and 40 mA. The morphology and structure of the products were characterized by a field emission scanning electron microscope (FESEM, Sirion 200 FEI) using an accelerating voltage of 5 kV and a transmission electron microscope (TEM, JEOL-2010, 200 kV) equipped with an energy-dispersive X-ray spectrometer (EDX, Oxford, Link ISIS). The specific surface areas of the samples were determined by nitrogen adsorption (Micrometrics ASAP 2020M) at 77 K using the Brunauer–Emmett–Teller (BET) equation. Photoluminescence (PL) measurement was performed using a LabRam confocal Raman microscope by JY Company. Samples were excited by the 325 nm line of a continuous He–Cd laser at room temperature. X-ray photo electron spectroscopic (XPS) analyses were conducted on a Thermo Scientific ESCALAB250Xi system equipped with a hemispherical energy analyser; an Al K_α X-ray source ($h\nu = 1486.6$ eV) was operated with a base pressure of 3×10^{-8} Pa.

Photocatalytic activity evaluation

The evaluation of photocatalytic performance for the removal of Cr(VI) in aqueous solutions was carried out at ambient condition. $K_2Cr_2O_7$ was used as the Cr(VI) source. 40 mg photocatalyst was added into 80 mL of 10 mg L^{-1} Cr(VI) solution. The pH value of the reaction suspension was adjusted to 2.5–8.0 using HCl or NaOH. Only the optimum pH was used in subsequent studies. Before irradiation, the solution was stirred for 30 min in the dark to reach adsorption–desorption equilibrium between the photocatalyst and Cr(VI) solution. A 300 W high-pressure mercury lamp with maximum emission of 365 nm was used as the UV light source. At a given time interval of irradiation, 3 mL of solution was taken out from the suspensions and centrifuged to remove the photocatalyst powder. The Cr(VI) concentration was monitored by the spectrophotometric method of diphenylcarbazide at 540 nm using a spectrophotometer (CARY-5E). The total Cr ion concentrations in the solutions were measured by an inductively coupled plasma-optical emission spectrophotometer (ICP 6000 Thermal Electron).

After the first cycle, all the photocatalysts, including the taken-out samples, were soaked in 10% HNO_3 solution for 5 h before washing several times with deionized water and ethanol. These were then dried at 70 °C for 8 h. The obtained powders were reused in the second and third cycles. The experimental process was similar to the above measurement of photocatalytic activity.

In another set of experiments, the evaluation of photocatalytic degradation for 20 mg L^{-1} (ppm) methyl orange and 50 mg L^{-1} 2,4-dichlorophenoxyacetic acid in water were performed using similar procedures. The concentrations of methyl orange and 2,4-dichlorophenoxyacetic acid were determined by the absorption peaks in UV-vis absorption spectra at the 464 and 282 nm peaks, respectively.

Results and discussion

Characterization of the as-synthesized F-THS and SF-THS

The morphologies of the as-synthesized TiO_2 hollow spheres (denoted by F-THS) are shown in Fig. 1. The field emission scanning electron microscope (FESEM) image (Fig. 1a) of F-THS shows that the sample contains large quantities of spheres with a diameter of ~1 μm. The partial broken sphere displayed its interior and confirmed that the spheres were hollow in structure. The high-magnification image of a single sphere (inset in Fig. 1a) shows that the external surface of the hollow sphere is rough and composed of randomly aggregated nanoflakes. The nanoflakes share a similar shape with the reactive (001) facet-exposed anatase single crystals, known as highly truncated tetragonal bipyramids (inset in Fig. 1b). The enlarged FESEM image of the surface of a single sphere (Fig. 1b) further confirmed the morphology of nanoflakes. The interfacial angles were determined to be around 68°, consistent with that between anatase (001) and (101) facets (inset in Fig. 1b). Thus, the outside surfaces of nanoflakes could be indexed as (001) facets of anatase, according to such shape symmetry. The transmission electron microscopy (TEM) image in Fig. 1c clearly reveals the hollow spherical architecture of F-THS, and the nanoflakes inlaid on the external surfaces can be observed from the enlarged image in the inset of Fig. 1c. In addition to shape symmetry, the corresponding selected-area electron diffraction (SAED) pattern and high-resolution TEM (HRTEM) are further presented to reveal the crystallographic orientation of nanoflakes, shown in Fig. 1d. The HRTEM image recorded perpendicular to the (001) facets shows a spacing of 0.19 nm, representing the {200} atomic planes of anatase TiO_2.[22–24] The above results suggest that the outside surfaces of the nanoflakes can be indexed as the reactive (001) facet of anatase. TiO_2 hollow spheres composed of smaller crystallite sizes (denoted as SF-THS) were also synthesized. The whole morphology of SF-THS (shown in Fig. S1†) is similar to that of F-THS, except that the building blocks of SF-THS are tiny nanoparticles with sizes ranging from about 10 to 20 nm, much smaller than the reactive (001) facet-exposed nanoflakes of F-THS.

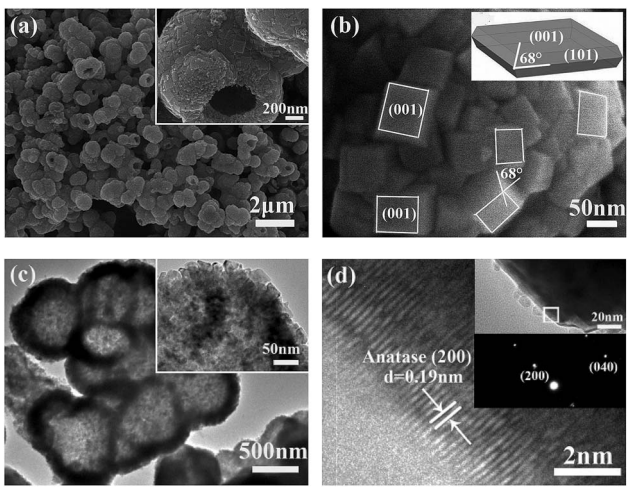

Fig. 1 (a and b) FESEM images of F-THS; inset in (a) is the high-magnification image of a single sphere, and (b) is the schematic model of a highly truncated tetragonal bipyramid exposing (001) facets, respectively. (c) TEM image of F-THS, inset is the enlarged image, and (d) HRTEM image and SAED pattern of the region highlighted by a rectangular box in the upper part of inset in (d).

The XRD patterns of F-THS and SF-THS are shown in Fig. 2a. All the peaks can be indexed as pure anatase phase of TiO_2 (JPCDS no. 21-1272). The peaks of F-THS are much narrower than that of SF-THS, indicating the increase in average crystal size, which is consistent with the FESEM and TEM observation. In order to study the internal pore structures and specific surface areas of F-THS and SF-THS, nitrogen adsorption–desorption measurement was performed (Fig. S2†). The isotherms of both F-THS and SF-THS are of type IV (Brunauer–Deming–Deming–Teller classification),[20] revealing the existence of abundant mesoporous structures. Using the BET equation, the specific surface area of F-THS and SF-THS were evaluated to be about 26 and 125 $m^2\ g^{-1}$, respectively. Fig. 2b shows the XPS survey spectrum of F-THS. In addition to the peaks of Ti, O and C (the C element is mainly ascribed to contamination from the XPS instrument itself and carbon dioxide in the air), a peak at 684.6 eV (Fig. 2c) was found, corresponding to that of F adsorbed on the surface of TiO_2 (≡Ti–F). No signal for F^- in the lattice of TiO_2 (bonding energy is equal to 688.5 eV) was detected.[21] The surface fluorination was caused by a simple ligand exchange reaction between surface hydroxyl groups on TiO_2 and fluoride anions (F^-) due to the high F–Ti bonding energy.[18]

Further study indicated that the molar ratio of fluorine to titanium (denoted by R_F) in the reaction solutions had a significant effect on the formation of F-THS (shown in Fig. S3†). When the value of R_F was equal to 0, *i.e.*, without the addition of fluoride, the products were solid spherical aggregates (Fig. S3a†). When R_F equaled to 0.5 or 1, a small amount of broken microspheres displaying hollow interior was observed (Fig. S3b and S3c†). When the R_F increased to 2, large quantities of hollow spheres similar to F-THS were obtained (Fig. S3d†). When the fluoride concentration further increased ($R_F = 5$), the product was solid microspheres composed of randomly aggregated nanoflakes (Fig. S3e†) instead of hollow microspheres. According to previous works by Yu *et al.*,[17,20,28] the formation of F-THS is a fluoride-mediated, self-transformation process, which has been proven to be an effective route for the synthesis of hollow sphere-structured TiO_2. Besides, the synthesis of anatase TiO_2 with (001) facets with the assistance of fluoride has also been reported.[22–24] In this work, proper fluoride concentration ($R_F = 3$)

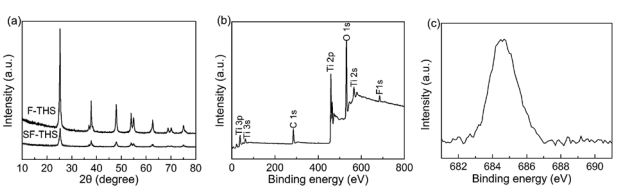

Fig. 2 (a) XRD patterns of the different samples, (b) XPS survey spectrum of F-THS and (c) high-resolution XPS spectrum of the F 1s region of F-THS.

not only favored the crystallization of anatase during the formation of the hollow sphere, but also induced the formation of reactive (001) facets.[22–24] Especially, the addition of urea tuned the nucleation dynamics of the elementary TiO_2 building blocks and inhibited the progressive crystal growth;[28] SF-THS was finally obtained and composed of small nanoparticles.

Optimal pH value on the photocatalytic removal of Cr(VI)

The influence of pH value on the photocatalytic activity of F-THS for Cr(VI) removal is shown in Fig. 3a. Cr(VI) was completely removed under UV light irradiation in 100 min at pH values of 2.5 and 4, while the removal efficiency of Cr(VI) decreased swiftly when the pH value increased over 4. The possible reason is that the potential difference between the conduction band of TiO_2 and Cr(VI)/Cr(III) increased with the decrease in pH; thus the thermodynamic driving force for the reduction of Cr(VI) was enhanced at low pH.[15] On the other hand, the zero charge point of TiO_2 is about pH = 6.25. In acidic condition, the surface of TiO_2 is mainly positively charged. Therefore, the lower pH was favourable for the adsorption of negatively charged Cr(VI) groups on TiO_2 due to electrostatic attraction, which consequently enhanced the Cr(VI) removal. In the high pH region, there was an electrostatic repulsion between the negatively charged group (CrO_4^{2-} or $Cr_2O_7^{2-}$) and TiO_2, resulting in a decrease in the adsorption.[13] It should be mentioned that the total Cr ion concentration in the solution measured by ICP did not decrease to zero under UV light irradiation for 100 min at the pH of 2.5 (Fig. 3b); there remained a total of 2.33 ppm Cr ions in the solution. This indicates that Cr(VI) ions were initially photocatalytically reduced to Cr(III) ions by F-THS, then desorbed into the solution due to the low adsorption capacity for Cr(III) on the surface of F-THS at this pH value.[29] However, desorption of Cr(III) ions was not found in the condition at pH = 4; the total concentration of Cr ions was found to be about 0.048 ppm after 100 min, which is slightly lower than the allowable limit of 0.05 ppm in the drinking water in countries like Sweden and Germany.[11] Based on the above results, we propose that the optimal pH value of the TiO_2 catalyst for the photocatalytic removal of Cr(VI) is around 4.

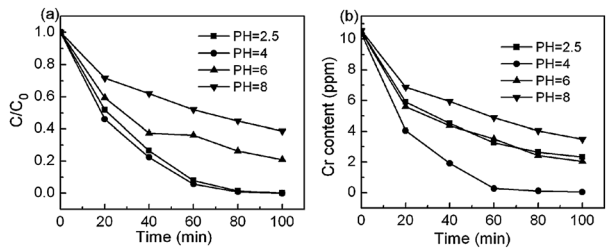

Fig. 3 (a) Cr(VI) normalization concentration and (b) the total Cr ion concentration in the solutions *versus* the exposure time under irradiation with the different initial pH values. C_0 is the initial concentration of Cr(VI); C is the concentration of the remaining Cr(VI) at time t. Cr(VI) concentration was measured by the spectrophotometric method of the diphenylcarbazide at 540 nm; the total Cr ion concentration was measured by an inductively coupled plasma (ICP)-optical emission spectrophotometer.

Effect of surface fluorination on the photocatalytic activity

The effect of fluorine on the photocatalytic activity of TiO_2 in the photodegradation of organic pollutants has been widely investigated;[17–21] however, its effect on the removal of heavy metal Cr(VI) has been rarely reported.[25] In order to investigate the influence of surface fluorination on the photocatalytic degradation of Cr(VI), the surface-bonded fluoride species of F-THS were removed by NaOH washing (see the Experimental section for details) without a change in morphology and structure; clean (001) facets were obtained as reported,[30,31] and the sample of F-THS after NaOH washing was denoted by THS. XPS was used to characterize the surface chemical compositions of F-THS and THS (Fig. 4a). It appears that the ratio of OH (at about 531.0 eV) to O^{2-} (at about 530.0 eV) in the O 1s spectra of THS increased more significantly than that of F-THS, indicating a replacement of the surface-bonded fluoride species by hydroxyl groups due to NaOH washing.[32] In addition, the photocatalytic activity of THS for the removal of Cr(VI) was investigated at pH = 4. The photocatalytic degradation rate of THS was found to be much faster than that of F-THS (Fig. 4b), demonstrating that surface fluorination hindered the photocatalytic activity. The result was contrary to previous reports that surface fluorination could significantly enhance the photocatalytic degradation of organic anionic, cationic, and neutral pollutants.[17–21] The photocatalytic activity of F-THS in the photodegradation of organic pollutants such as methyl orange and 2,4-dichlorophenoxyacetic acid was hindered after the removal of the surface fluorination by NaOH washing (shown in Fig. S4†), indicating that surface fluorination was indeed beneficial to the photocatalytic degradation of the organic pollutant. The negative role of surface fluorination for the photocatalytic removal of Cr(VI) might have originated from the following two sources. First, there were more surface THS hydroxyl groups due to the replacement of the surface-bonded fluoride species by NaOH washing, and this might have played a decisive role in the photocatalytic reduction removal of Cr(VI).[25,32] Second, it has been reported that surface Ti–F groups can act as electron-trapping sites to trap the photo-generated electrons and transfer them to the O_2 adsorbed on the surface of TiO_2, thus enhancing the separation of electrons and holes.[20,33] In our work, the effect of fluorination on the recombination of photo-generated electron/hole pairs of the samples was measured by PL emission (shown in Fig. 4c). The intensity of PL

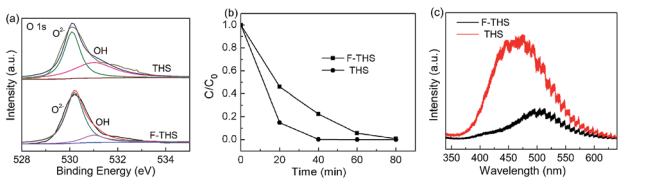

Fig. 4 (a) High-resolution XPS spectra of O 1s region of the different TiO_2 powders, (b) Cr(VI) normalization concentration *versus* the exposure time under irradiation with the different TiO_2 photocatalysts. C_0 is the initial concentration of Cr(VI); C is the concentration of the remaining Cr(VI) at time t. (c) Photoluminescence spectra of the different TiO_2 powders.

spectra of F-THS was much lower than that of THS, indicating that a better separation efficiency of electrons and holes can indeed be achieved by surface fluorination.[14] However, the difference was that the photocatalytic degradation of organic pollutants mainly relied on the photo-generated holes, while the photocatalytic reduction of Cr(VI) needed the participation of photo-generated electrons. The trapping of photo-generated electrons by the surface Ti–F group hindered the transfer of electrons to Cr(VI), and thus was detrimental to the photocatalytic reduction of Cr(VI). Our result is different from the previous work, which reported that surface fluorination was beneficial to the photocatalytic removal of Cr(VI),[25] because part of the surface-bonded fluoride species in that work was substitutional F atoms in TiO_2 crystal lattice; however, in this work, the surface-bonded fluoride species was wholly surface-absorbed F(≡Ti–F). Investigative work also showed that a similar experiment on the photocatalytic activity of SF-THS for degradation of Cr(VI) is enhanced after removal of surface fluorination by NaOH washing (Fig. S5,† the sample of the SF-THS after NaOH washing is denoted by S-THS). All the above results point to the fact that surface fluorination of TiO_2 hollow spheres hinders the photocatalytic removal of Cr(VI).

Structurally enhanced photocatalytic activity

The photocatalytic activity of the commercial anatase micron-sized and nanometer-sized TiO_2 powders (see Fig. S6†) was selected as the standard references in the evaluation of the removal ability for Cr(VI). Fig. 5 shows the photocatalytic performance for the Cr(VI) removal with the different TiO_2 photocatalysts at the pH level of 4. Without the addition of photocatalyst, Cr(VI) removal could not be observed under irradiation (curve (I) in Fig. 5). The THS and S-THS with hierarchical structure exhibited higher photocatalytic activity than that of mono-morphological commercial anatase micron-sized and nanometer-sized TiO_2 powders, as shown in Fig. 5. At relatively low Cr(VI) concentration, their photocatalytic process and reaction kinetics can be expressed by a pseudo-first-order reaction and an apparent rate constant k_{app} (shown in Table 1). The k_{app} of THS was nearly 6 and 18 times larger than that of the nanometer-sized TiO_2 and micron-sized TiO_2, respectively. The k_{app} of S-THS was also larger than that of the nanometer-sized TiO_2 and micron-sized TiO_2 by a factor of about 3 and 6 times, respectively. This enhanced photocatalytic performance of THS and S-THS could be described as structure-induced enhancement,[34,35] attributed to the high specific surface area and abundant mesoporous properties of the TiO_2 hollow spheres, which provide ideal channels for easy and fast diffusion of the Cr(VI) molecules to contact the TiO_2 building blocks.[34] Moreover, the enhanced light harvesting abilities owing to the special hollow structures of THS and S-THS increase the quantity of photo-generated electrons and holes to participate in the photocatalytic reactions.[16] Also, we have presented the systematic comparison experiment to study the photocatalytic efficiency of the commercial photocatalyst Degussa P25 (see Fig. S7 in the ESI†); it was found that the photocatalytic efficiency of Degussa P25 was much lower than that of the as-synthesized hierarchical structure TiO_2 hollow spheres, indicating enhanced activity of the TiO_2 hollow spheres in the photocatalytic removal of Cr(VI).

The morphology of THS before and after treating the Cr(VI) solution was examined by TEM (Fig. S8a†); there was no obvious morphology change in the hollow sphere structure. The element analysis using energy dispersive X-ray spectrometer (EDX) revealed that Ti, Cr, O, C and Cu elements co-existed on the surface of THS after treatment of the Cr(VI) solution (Fig. S8b†). Among them, Ti and O signals originated from TiO_2 crystals; the C signal was from the carbon film; Cu was from the copper grid. The spatial distribution of the different compositional elements was clarified by elemental mapping (Fig. S8c–S8e†). The spatial distribution of Cr is similar to the distribution of Ti and O, indicating that THS is an effective photocatalyst for the removal of Cr(VI).

It is worth noting that THS showed the best photocatalytic performance, but its specific surface area was much lower than that of S-THS and nanometer-sized TiO_2 powders (shown in Table 1). This indicated that specific surface area is an important factor influencing the photocatalytic activity, but is not the only one. Since THS and S-THS had similar preparation conditions and morphology, the presence of reactive (001) facets in THS might contribute significantly to its observed high photocatalytic activity. Reactive (001) facets of THS with 100% five coordinate unsaturated linkage Ti atoms (5c-Ti) are more beneficial to the absorption of negatively charged Cr(VI),[36] in contrast to the normally exposed (101) facets with only 50% unsaturated linkage Ti atoms (Fig. 6). Besides, according to some previous reports,[22,25] the synergism of reactive (001) facets and (101) facets in THS might induce the selective migration of photo-generated electrons and holes to the specific exposed crystal facets, which would hinder the recombination rate of

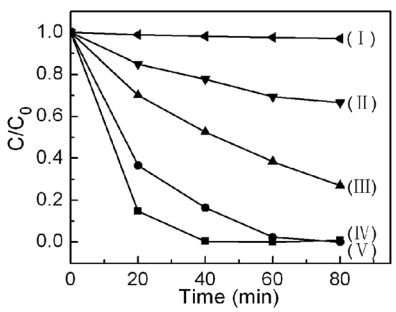

Fig. 5 Cr(VI) normalization concentration *versus* the exposure time under irradiation with the different TiO_2 catalysts: (I) without catalysts; (II) micron-sized TiO_2 powder; (III) nanometer-sized TiO_2 powder; (IV) S-THS and (V) THS.

Table 1 BET specific surface area and apparent rate constant data k_{app} of the different TiO_2 photocatalysts

Sample	THS	S-THS	Micron-sized TiO_2	Nanometer-sized TiO_2
BET ($m^2\ g^{-1}$)	26	125	2.2	60
k_{app} (min^{-1})	0.0867	0.0516	0.0051	0.0161

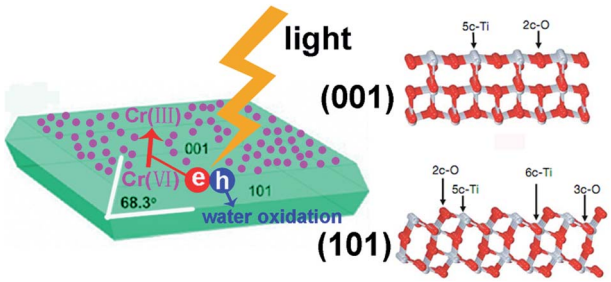

Fig. 6 Schematic illustration of the photocatalytic removal of Cr(VI) with reactive (001) facets and the atomic structures of clean (001) and (101) surfaces. Cr(VI) molecules are represented by purple spheres. Ti and O atoms are represented by grey and red spheres, with six-fold Ti, five-fold Ti, three-fold O and two-fold O labelled as 6c-Ti, 5c-Ti, 3c-O and 2c-O, respectively.

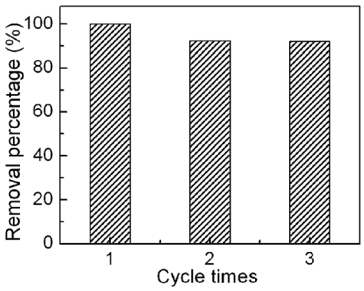

Fig. 7 Durability of THS under UV light irradiation for the three cycles.

photo-generated electrons and holes and thus enhance photocatalytic activity (Fig. 6). In the present study, we found that the F-THS with reactive (001) facets showed much lower dark adsorption ability of Cr(VI) than SF-THS. After 30 min of dark adsorption for F-THS and SF-THS, the Cr(VI) removal efficiencies were 1.6% and 5.3%, respectively, due to the surface fluorination that hindered the activity of (001) facets. When the surface fluorination was removed through NaOH washing, the excellent adsorption ability of THS with clean reactive (001) facets was fully reflected, exceeding that of S-THS (the Cr(VI) removal efficiencies after 30 min of dark adsorption for THS and S-THS were 9.8% and 7.1%, respectively). The results indicate that reactive (001) facets are indeed more beneficial to the absorption of negatively charged Cr(VI). Moreover, reactive (001) facet-exposed nanosheets were also synthesized by the previous method[37] and used to investigate the activity of the different crystal facets in the photocatalytic removal of Cr(VI) compared to THS. Fig. S9† shows the TEM images of the nanosheets after treating the Cr(VI) solution; there were many Cr species wrapped around the nanosheets, especially around the (001) facets (Fig. S9c†). The Cr species contents were analyzed by EDX; the content of Cr species absorbed on the (001) facets (EDX recorded from [001] direction) was about three times higher than that of the (101) facets (EDX recorded from [100] direction), indicating that the reactive (001) facets indeed had higher activity in the photocatalytic removal of Cr(VI). The detailed evidence is under investigation.

XPS was used to further study the adsorbed Cr species on the surface of THS after photocatalytic reaction. Fig. S10† shows the corresponding high-resolution XPS spectra of the Cr 2p region. The broad peak of Cr $2p^{3/2}$ can be fitted to two main peaks of 576.5 and 577.6 eV, consistent with the reported XPS spectra for oxides or the hydroxide of characteristic Cr(III) (*e.g.* $Cr(III)_xO_y$ and $Cr(OH)_3$); a weak peak at 579.6 eV corresponded to the characteristic binding energy of adsorbed Cr^{6+} ions.[38,39] This suggests that the photocatalytic process of Cr(VI) is as follows: Cr(VI) ions are first adsorbed on the surface of THS, then reduced to Cr(III) species by the photo-excited electrons, and finally deposited on the surface of THS.

The capacity of photocatalyst THS for the removal of Cr(VI) was also investigated (Fig. S11†). The removal efficiency still reached 50% and 70% after 4 h of UV light irradiation with 0.1 and 0.3 g L^{-1} THS, respectively, indicating that each gram of THS can eliminate up to 50 mg of Cr(VI) from water. It is higher than that of the reported Fe_3O_4 micron-spheres and mesoporous titanium beads,[16,32] and the removal time here is much shorter.

In addition to photocatalytic activity, the stability and recyclability of the photocatalyst are also important in practical applications. In the present study, the durability of the photocatalytic activity of THS was studied by reusing the catalysts in fresh Cr(VI) solution under the UV light irradiation. Fig. 7 shows the photocatalytic ability of THS for three cycles (40 min irradiation for each cycle). The removal percentage of Cr(VI) after three cycles still reached 92%, indicating the feasibility of regeneration of THS.

Conclusions

Hierarchical structure TiO_2 hollow spheres with reactive (001) facets were hydrothermally synthesized with a high yield based on a fluoride-mediated, self-transformation strategy. Evaluation of the photocatalytic removal of heavy metal Cr(VI) suggests that surface fluorination of TiO_2 hollow spheres plays a negative role against photocatalytic activity. When the surface fluorine of TiO_2 hollow spheres was removed, a considerably enhanced photocatalytic activity was achieved compared to the other structured TiO_2 powders; the hierarchical structure (high specific surface area and abundant mesoporous properties) together with the reactive (001) facets contributed to the enhanced photocatalytic activity. Further characterization results suggested that TiO_2 hollow spheres not only removed Cr(VI) from the wastewater, but also reduced the adsorbed toxic Cr(VI) to less toxic Cr(III) and further formed oxide or hydroxide products. Moreover, TiO_2 hollow spheres can be regenerated. This work not only enriches the application of TiO_2 hollow spheres in the photocatalytic treatment of Cr(VI), but also reveals the double-sided nature of the surface fluorination. However, the relationship between the exposed reactive (001) facets and the enhanced photocatalytic activity towards Cr(VI) needs to be further studied. The as-synthesized hierarchical structure TiO_2 hollow spheres are also of great interest in the removal of other environmental pollutants.

Acknowledgements

This work was supported by the National Basic Research Program of China (Grant no. 2013CB934302), the Natural Science Foundation of China (Grant no. 51072199, 21177132 and 51272255), and Strategic Priority Research Program of the Chinese Academy of Sciences (Grant no. XDA09030200).

Notes and references

1 S. X. Liu, *Bull. Environ. Contam. Toxicol.*, 2005, **74**, 706.
2 L. M. Wang, N. Wang, L. H. Zhu, H. W. Yu and H. Q. Tang, *J. Hazard. Mater.*, 2008, **152**, 93.
3 M. Rivero and W. D. Marshall, *J. Hazard. Mater.*, 2009, **169**, 1081.
4 M. V. Dozzi, A. Saccomanni and E. Selli, *J. Hazard. Mater.*, 2012, **211**, 188.
5 R. L. Qiu, D. D. Zhang, Z. H. Diao, X. F. Huang, C. He, J. L. Morel and Y. Xiong, *Water Res.*, 2012, **46**, 2299.
6 X. W. Zhao and L. M. Qi, *Nanotechnology*, 2012, **23**, 235604.
7 Y. Q. Xing, X. M. Chen and D. H. Wang, *Environ. Sci. Technol.*, 2007, **41**, 1439.
8 I. Heidmann and W. Calmano, *J. Hazard. Mater.*, 2008, **152**, 934.
9 P. Gao, X. M. Chen, F. Shen and G. H. Chen, *Sep. Purif. Technol.*, 2005, **43**, 117.
10 R. Guell, E. Antico, V. Salvado and C. Fontas, *Sep. Purif. Technol.*, 2008, **62**, 389.
11 S. Mor, K. Ravindra and N. R. Bishnoi, *Bioresour. Technol.*, 2007, **98**, 954.
12 M. E. R. Carmona, M. A. P. Silva and S. G. F. Leite, *Process Biochem.*, 2005, **40**, 779.
13 J. W. Fan, X. H. Liu and J. Zhang, *Environ. Technol.*, 2011, **32**, 427.
14 X. J. Liu, L. K. Pan, T. Lv, G. Zhu, T. Lu, Z. Sun and C. Q. Sun, *RSC Adv.*, 2011, **1**, 1245.
15 J. K. Yang, S. M. Lee, M. Farrokhi, O. Giahi and M. S. Siboni, *Desalin. Water Treat.*, 2012, **46**, 375.
16 G. Liu, Q. Deng, H. M. Wang, S. H. Kang, Y. Yang, D. H. L. Ng, W. P. Cai and G. Z. Wang, *Chem.–Eur. J.*, 2012, **18**, 13418.
17 J. G. Yu, S. W. Liu and H. G. Yu, *J. Catal.*, 2007, **249**, 59.
18 J. Q. Li, D. F. Wang, H. I. Liu, Z. L. He and Z. F. Zhu, *Appl. Surf. Sci.*, 2011, **257**, 5879.
19 J. G. Yu and J. Zhang, *Dalton Trans.*, 2010, **39**, 5860.
20 J. G. Yu, Q. J. Xiang, J. R. Ran and S. Mann, *CrystEngComm*, 2010, **12**, 872.
21 M. Liu, K. L. Lv, G. H. Wang, Z. Y. Wang, Y. X. Zhao and Y. R. Deng, *Chem. Eng. Technol.*, 2010, **33**, 1531.
22 S. W. Liu, J. G. Yu and M. Jaroniec, *Chem. Mater.*, 2011, **23**, 4085.
23 D. Q. Zhang, G. S. Li, X. F. Yang and J. C. Yu, *Chem. Commun.*, 2009, 4381.
24 H. G. Yang, C. H. Sun, S. Z. Qiao, J. Zou, G. Liu, S. C. Smith, H. M. Cheng and G. Q. Lu, *Nature*, 2008, **453**, 638.
25 Z. Q. He, Q. L. Cai, M. Wu, Y. Q. Shi, H. Y. Fang, L. D. Li, J. C. Chen, J. M. Chen and S. Song, *Ind. Eng. Chem. Res.*, 2013, **52**, 9556.
26 S. J. Ding, J. S. Chen, Z. Y. Wang, Y. L. Cheah, S. Madhavi, X. A. Hu and X. W. Lou, *J. Mater. Chem.*, 2011, **21**, 1677.
27 X. L. Wang, H. L. He, Y. Chen, J. Q. Zhao and X. Y. Zhang, *Appl. Surf. Sci.*, 2012, **258**, 5863.
28 S. W. Liu, J. G. Yu and S. Mann, *Nanotechnology*, 2009, **20**, 325606.
29 S. C. Xu, Y. X. Zhang, S. S. Pan, H. L. Ding and G. H. Li, *J. Hazard. Mater.*, 2011, **196**, 29.
30 S. W. Liu, J. G. Yu and M. Jaroniec, *J. Am. Chem. Soc.*, 2010, **132**, 11914.
31 Z. Y. Wang, K. L. Lv, G. H. Wang, K. J. Deng and D. G. Tang, *Appl. Catal., B*, 2010, **100**, 378.
32 N. Wu, H. H. Wei and L. Z. Zhang, *Environ. Sci. Technol.*, 2012, **46**, 419.
33 J. G. Yu, W. G. Wang, B. Cheng and B. L. Su, *J. Phys. Chem. C*, 2009, **113**, 6743.
34 X. W. Duan, G. Z. Wang, H. Q. Wang, Y. Q. Wang, C. Shen and W. P. Cai, *CrystEngComm*, 2821, **2010**, 12.
35 F. Lu, W. P. Cai and Y. G. Zhang, *Adv. Funct. Mater.*, 2008, **18**, 1047.
36 J. Pan, G. Liu, G. Q. Lu and H. M. Cheng, *Angew. Chem., Int. Ed.*, 2011, **50**, 2133.
37 Z. Y. Wang, K. L. Lv, G. H. Wang, K. J. Deng and D. G. Tang, *Appl. Catal., B*, 2010, **100**, 378.
38 M. Mullet, F. Demoisson, B. Humbert, L. J. Michot and D. Vantelon, *Geochim. Cosmochim. Acta*, 2007, **71**, 3257.
39 D. Shuttleworth, *J. Phys. Chem.*, 1980, **84**, 1629.